ADVANCING EARTH AND SPACE SCIENCES

Geophysical Research Letters

RESEARCH LETTER
10.1029/2026GL122115

Key Points:
- A U-Net model reconstructs 950-hPa winds from satellite sea surface winds over the South China Sea
- The reconstructed winds outperform ERA5 when evaluated against independent shipborne observations
- The reconstruction reduces ERA5 underestimation of marine boundary layer jet intensity

Correspondence to:
Y. Du and J. Wang,
duyu7@mail.sysu.edu.cn;
Wangjk57@mail.sysu.edu.cn

Citation:
Lin, Y., Du, Y., & Wang, J. (2026). Reconstructing marine boundary layer jets over the South China Sea using machine learning. *Geophysical Research Letters*, *53*, e2026GL122115. https://doi.org/10.1029/2026GL122115

Received 27 JAN 2026
Accepted 1 MAY 2026

Author Contributions:
Conceptualization: Yu Du, Jiuke Wang
Data curation: Yican Lin, Yu Du, Jiuke Wang
Formal analysis: Yican Lin
Funding acquisition: Yu Du
Investigation: Yican Lin
Methodology: Yican Lin
Project administration: Yu Du
Resources: Yu Du
Software: Yican Lin
Supervision: Yu Du, Jiuke Wang
Validation: Yican Lin
Visualization: Yican Lin
Writing – original draft: Yican Lin
Writing – review & editing: Yican Lin, Yu Du, Jiuke Wang

Reconstructing Marine Boundary Layer Jets Over the South China Sea Using Machine Learning

Yican Lin[1], Yu Du[1,2,3], and Jiuke Wang[4]

[1]School of Atmospheric Sciences, Sun Yat-sen University, and Southern Marine Science and Engineering Guangdong Laboratory (Zhuhai), Zhuhai, China, [2]Guangdong Province Key Laboratory for Climate Change and Natural Disaster Studies, Sun Yat-sen University, Zhuhai, China, [3]Key Laboratory of Tropical Atmosphere-Ocean System, Sun Yat-sen University, Ministry of Education, Zhuhai, China, [4]School of Artificial Intelligence, Sun Yat-sen University, and Southern Marine Science and Engineering Guangdong Laboratory (Zhuhai), Ministry of Education, Zhuhai, China

Abstract Marine boundary layer jets (MBLJs) over the South China Sea (SCS) play a critical role in coastal heavy rainfall, yet their structure remains uncertain due to limited wind observations over the ocean. Here, we develop a U-Net–based reconstruction framework to estimate 950-hPa winds from satellite-derived sea surface winds, providing a satellite-driven depiction of MBLJs. The model is trained using four decades of ERA5 data and evaluated against independent shipborne Doppler wind LiDAR observations. Relative to ERA5, the reconstructed winds reduce RMSE from 3.34 to 2.69 m s^{-1} for wind speed and from 2.87 to 2.45 m s^{-1} for meridional wind. During identified MBLJ events, the reconstruction produces stronger and more spatially extensive jets than ERA5. These results demonstrate that satellite-informed machine learning can effectively mitigate systematic underestimation of MBLJs in reanalysis products and improve representation of boundary-layer winds over data-sparse oceanic regions.

Plain Language Summary Over the South China Sea, fast-moving low-level winds, called marine boundary layer jets (MBLJs), often trigger heavy rainfall along the coast of southern China. Direct measurements of these winds over the ocean are rare, leaving their strength and vertical structure poorly understood. As a result, weather models often struggle to represent MBLJs accurately, leading to errors in coastal rainfall forecasts. In this study, we use a deep learning model to estimate winds a few hundred meters above the ocean by using satellite observations of surface winds. When tested against ship-based wind measurements, the new method performs better than a widely used weather data set (ERA5), especially in capturing the strength of these jets. This approach provides a practical way to map low-level winds over large ocean areas where traditional observations are scarce.

1. Introduction

Boundary layer jets (BLJs) are strong low-level wind maxima that form below ~1 km in altitude, typically exceeding 10 m s^{-1} (Du & Rotunno, 2014; Stensrud, 1996). Characterized by pronounced vertical wind shear and a distinct nocturnal intensification, BLJs frequently develop over the northern South China Sea and play a crucial role in modulating coastal and inland rainfall across South China (Du & Chen, 2018, 2019; X. Zhang et al., 2024). By transporting warm, moist air inland and enhancing low-level convergence, marine BLJs (MBLJs) provide favorable dynamical and thermodynamic conditions for the initiation and intensification of rainfall (Chen et al., 2017; Du et al., 2022; Du & Chen, 2019; Fu et al., 2025; Luo & Du, 2023; H. Yang et al., 2025).

Most previous studies of MBLJs rely primarily on reanalysis data sets, particularly ERA5 (Du & Yi, 2025; Z. Li et al., 2020; Luo & Du, 2023). However, shipborne observations over the South China Sea indicate that reanalysis products substantially underestimate both the frequency and intensity of MBLJs due to the scarcity of direct low-level wind measurements over the ocean (Zhang et al., 2024). These deficiencies propagate errors into numerical model initializations and forecasts (Y. Lin & Du, 2025; M. Zhang & Meng, 2019; X. Zhang et al., 2024). Although recent advances in satellite wind retrieval, such as Europe's Aeolus mission employing active LiDAR measurements and the derivation of atmospheric motion vectors (AMVs) from passive sensors, improve tropospheric wind monitoring, both approaches remain inadequate for resolving MBLJs. Aeolus suffers from limited accuracy near the surface (Lukens et al., 2022; Witschas et al., 2020), while AMVs exhibit uncertainties in wind height assignment and cloud tracking (Ma et al., 2021; Velden & Bedka, 2009). This persistent observational gap motivates the development of novel approaches to reconstruct low-level winds over oceanic regions, which is essential for achieving a more realistic depiction of MBLJs and their associated impacts.

Scatterometer-derived sea surface winds provide a valuable constraint on low-level dynamics (Mears et al., 2022). These instruments transmit microwave pulses, typically in the C- or Ku-band, toward the sea surface and retrieve surface wind speed and direction from the backscattered signals caused by surface roughness (Fetterer et al., 2002). With reasonable retrieval accuracy (Z. Wang et al., 2021; X. Yang et al., 2011), scatterometer data are widely used in weather forecasting, oceanography research, and climate monitoring (Atlas et al., 2001; Chang et al., 2009; Chelton et al., 2006). Because atmospheric fields are spatially continuous, sea surface winds are generally correlated with winds aloft, as governed by boundary-layer dynamics (C. Lin et al., 2013; Shreffler, 1982). However, the vertical separation between the ocean surface and the typical height of MBLJs near 950 hPa introduces a highly nonlinear relationship that is difficult to express analytically. Nevertheless, the potential to infer boundary-layer wind structures from sea surface winds remains significant but largely unexplored, motivating the development of data-driven machine learning approaches to bridge this gap.

Recent advances in artificial intelligence (AI) have enabled reconstruction of complex nonlinear atmospheric fields, from global forecasting systems to high-resolution field mapping (Bi et al., 2023; Sun et al., 2025; Xie et al., 2022). Building on these developments, this study proposes a deep learning framework to reconstruct MBLJs over the South China Sea using satellite-derived sea surface wind observations. The framework learns the physical linkage between surface and boundary-layer winds, providing improved estimates of low-level wind structures that are often misrepresented in reanalysis. By integrating satellite observations and reanalysis data, the approach bridges the observational gap over the ocean and enhances depictions of MBLJ intensity and spatial distribution. The reconstructed wind fields are validated against independent observations to assess their ability to capture essential dynamical features of MBLJs.

2. Data

2.1. Reanalysis Data

ERA5 reanalysis data (1979–2024) were employed for model training, validation, and testing. Data from 1979 to 2016 were used for training, 2017 to 2020 for validation, and 2021 to 2024 for testing. This temporal division was adopted to reduce cross-set correlations, given strong spatial and temporal autocorrelations in atmospheric variables. Input variables consist of 10-m zonal (u) and meridional (v) wind components, and outputs are the corresponding u and v wind components at 950 hPa. The ERA5 data set provides wind fields at a horizontal resolution of $0.25° \times 0.25°$ and 1-hr temporal resolution (Hersbach et al., 2018).

2.2. Satellite Data

The satellite-derived sea surface wind data used in this study are Level 2B near-real-time wind vectors from the HY-2B microwave scatterometer (M. Lin et al., 2013; X. Wang et al., 2012; Xing et al., 2016). The data set has a spatial resolution of 25×25 km and provides twice-daily global coverage. Winds are retrieved using the maximum likelihood estimation method, with an accuracy of 2 m s^{-1} or 10% for wind speed (X. Li et al., 2022). The data were obtained from the National Satellite Ocean Application Service (NSOAS). To ensure data quality, retrievals contaminated by rainfall and flagged as unreliable were excluded. These satellite wind observations were not assimilated into any reanalysis data sets and were not used during model training; instead, they were employed as independent inputs to assess model performance in practical applications.

2.3. Research Vessel Data

Shipborne LiDAR data from the research vessel Tan Kah Kee were used for independent validation. The LiDAR provides vertical wind profiles at ~25-m vertical resolution and 5-min temporal resolution. Observations correspond to a May–June 2021 cruise covering the northern South China Sea, where MBLJs frequently occur.

In addition, radiosonde observations launched from the Sun Yat-sen University research vessel were included. Balloons were released every six hours from 14:00 LST on 15 June to 08:00 LST on 16 June, and every three hours from 14:00 LST on 17 June to 23:00 LST on 18 June, during a scientific expedition conducted from 15 to 18 June 2022.

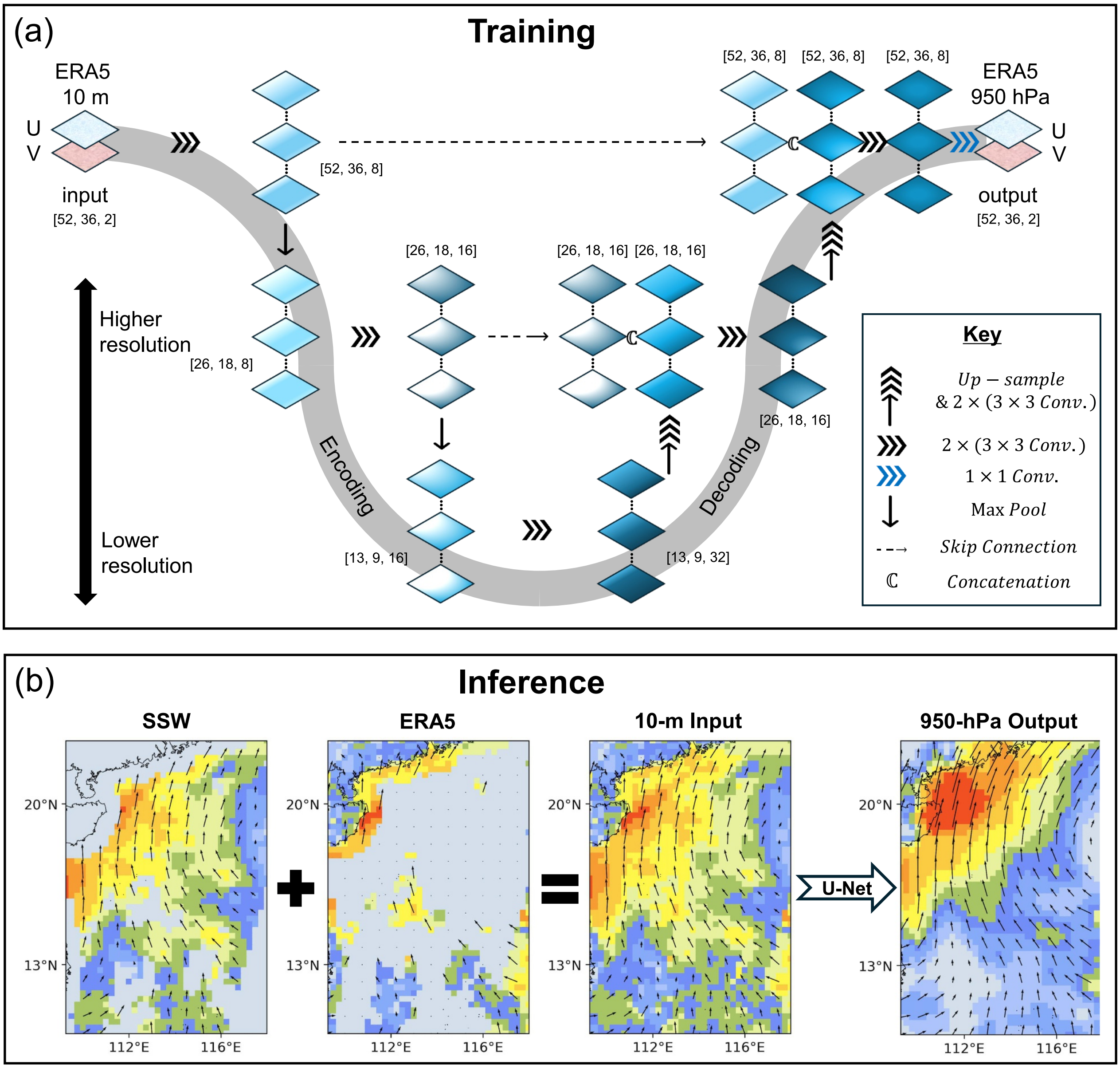

Figure 1. (a) Architecture of the U-Net model used to reconstruct boundary-layer winds. (b) Workflow for generating 950-hPa wind fields from satellite-derived sea surface winds (SSW) and ERA5 10-m winds. The model architecture is adapted from Chase et al. (2023).

These in situ observations were not assimilated into any reanalysis data sets and were not used in model training, ensuring their independence for validation. To ensure temporal and spatial consistency with model outputs, all observations and ERA5 reanalysis were matched within ±30 min of the satellite overpass. Only observations closest to the 950-hPa level were selected for comparison.

2.4. Domain of Interest

The analysis domain covers the northern South China Sea (Figure 1b), encompassing the primary hotspot of southerly MBLJs (Du et al., 2022) and the coastal–offshore environment relevant to MBLJ formation. Satellite-based reconstruction and model–observation comparisons are confined to this region. Within this broader region, MBLJ events are identified over a focused subregion (18–21°N, 111–113°E), corresponding to the core hotspot of southerly MBLJs. Detailed identification criteria are provided in Section 3.4.

3. Methods

3.1. Deep Learning Framework

This study employs a U-Net-based deep learning framework to reconstruct boundary-layer winds from surface winds. U-Net is a widely used convolutional neural network (CNN) architecture known for its strong capability in spatial feature extraction and multiscale representation (Gu et al., 2018; LeCun & Bengio, 1998). U-Net is a modified fully convolutional network that maps input images to output images of the same size through a symmetric encoder–decoder structure (Ronneberger et al., 2015). This architecture effectively captures both local and large-scale spatial dependencies, making it well suited for our objective of mapping surface (10 m) wind fields to their corresponding boundary-layer (950 hPa) winds.

3.2. Model Architecture and Training

The U-Net architecture is illustrated in Figure 1a. The inputs consist of the *u* and *v* components of 10-m winds. The encoder includes two stages of downsampling, each with two convolutional layers followed by activation functions and a max-pooling operation. The decoder mirrors this structure through two upsampling stages, including convolutional and activation layers, as well as skip connections to retain fine-scale spatial information removed during downsampling. A final 1×1 convolution layer produces two output channels representing the 950-hPa *u* and *v* components.

All input and output variables are normalized to improve training stability and convergence. The model is trained with a batch size of 64 using the Adam algorithm and the Huber loss function, which is less sensitive to outliers and well suited for geophysical data sets (Xie et al., 2022). To further enhance training efficiency, a ReduceLROnPlateau learning-rate scheduler is applied to dynamically adjust the learning rate when the validation loss plateaus, using a reduction factor of 0.5 and a patience of 5 epochs.

3.3. Inference With Satellite and Reanalysis Inputs

After training, the model performs inference using a combination of satellite-derived and ERA5 10-m winds. HY-2B scatterometer observations provide sea surface wind vectors retrieved using a maximum-likelihood estimation algorithm. HY-2B winds are bilinearly interpolated to the ERA5 grid to ensure spatial consistency. Given directional uncertainties in scatterometer winds, only wind speeds from HY-2B are used, while wind directions are taken from ERA5. Data gaps, resulting from rain-contaminated observations and from reduced data availability over land and coastal regions due to orbital sampling limitations, were filled using ERA5 wind fields from the closest temporal match. The trained U-Net then reconstructs the corresponding 950-in the representation hPa winds (Figure 1b).

3.4. Criteria for Identifying MBLJs

MBLJs are identified following established criteria (Du & Chen, 2019; Du & Rotunno, 2014; Du et al., 2022; Tu et al., 2019):

1. Maximum wind speed exceeds 10 m s^{-1} within the lowest 100-hPa layer above the surface;
2. Wind speed decreases by at least 3 m s^{-1} from the jet-level maximum to the minimum above it, below 600 hPa.
3. The meridional wind component at the jet core level is positive.

Over the northern South China Sea (18°–21°N, 111°–113°E), an MBLJ event is defined when >50% of grid points satisfy the above criteria, with no minimum duration required.

4. Results and Discussion

4.1. Model Performance

We first evaluate the trained model on the test data set to assess both its ability to capture the learned relationships and its generalization to unseen samples. Overall, the model demonstrates stable convergence and strong predictive skill across all evaluation cases.

As shown in Figure 2, the reconstructed 950-hPa wind fields closely match the reference data for wind speed and the *u* and *v* components. This demonstrates that the U-Net successfully learns the nonlinear mapping between the

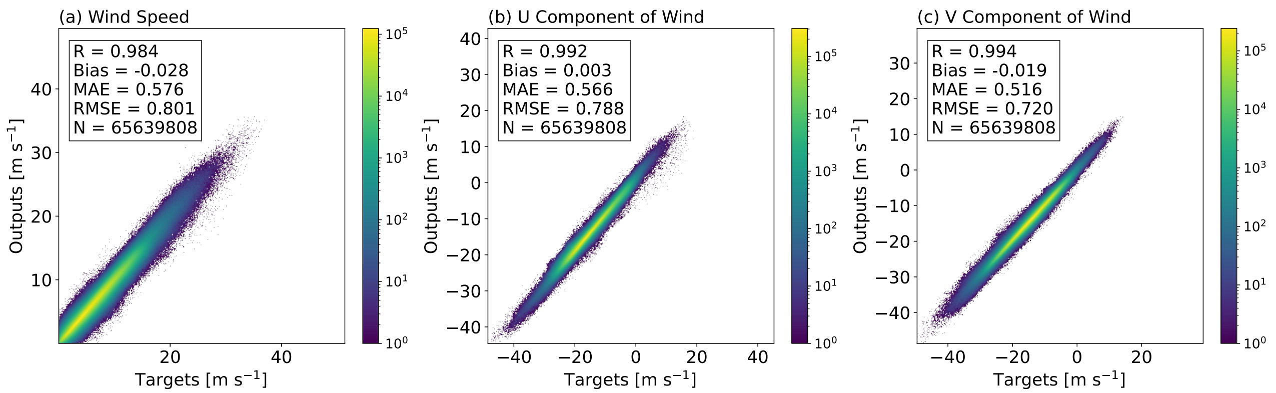

Figure 2. Density scatter plots comparing model outputs with target values for (a) wind speed, (b) u component, and (c) v component at 950 hPa in the test set (ERA5 reanalysis data from 2021 to 2024). Statistical metrics include the correlation coefficient (R), bias, mean absolute error (MAE), and root-mean-square error (RMSE). The sample size is $N = 65{,}639{,}808$.

10-m surface winds and boundary-layer winds. The correlation coefficients exceed 0.99 for both u (0.992) and v (0.994), and reach 0.984 for wind speed, indicating excellent agreement between predictions and targets. Mean bias error (MBE) values are very small (<0.03 m s^{-1}), with u bias nearly zero (0.003 m s^{-1}). Mean absolute error (MAE) values remain below 0.6 m s^{-1}, and RMSE values stay below 0.8 m s^{-1}. Because wind speed is a nonlinear combination of u and v, its errors are slightly larger than those of the individual components.

These results confirm that the model reliably reconstructs the 950-hPa wind field and performs robustly across the full test data set. While the evaluation using reanalysis data demonstrates strong model skill, assessing real-world applicability requires driving the model with satellite-observed sea surface winds and validating the reconstructed winds against independent measurements. The next section presents these results.

4.2. Independent Validation Using Observations

Figure 3 compares the U-Net-reconstructed winds, ERA5 reanalysis, and independent observations at 950 hPa. Overall, all three data sets exhibit similar variability from case to case. However, the U-Net reconstruction more closely follows the observed evolution than ERA5, particularly for the v component and total wind speed.

A quantitative evaluation further confirms these improvements. Relative to ERA5, the U-Net model consistently exhibits reduced errors in both wind components. For the u component, RMSE value decreases from 3.38 m s^{-1} (ERA5) to 2.91 m s^{-1}, while MAE value declines from 2.43 m s^{-1} to 2.33 m s^{-1}, indicating improved representation of zonal wind variability. Similarly, for the v component, RMSE value is reduced from 2.87 m s^{-1} to 2.45 m s^{-1} and MAE value from 2.30 m s^{-1} to 1.88 m s^{-1}, reflecting a substantial improvement in the representation of meridional wind variability. Wind speed errors are also reduced, with RMSE value decreasing from 3.34 m s^{-1} to 2.69 m s^{-1} and MAE value from 2.37 m s^{-1} to 2.08 m s^{-1}. The improvement is most pronounced under stronger wind conditions (>5 m s^{-1}), where U-Net predictions show closer agreement with observations than ERA5, highlighting the model's enhanced capability in capturing high-wind regimes. In addition, correlation coefficients are consistently higher for U-Net than for ERA5 across all variables, indicating improved consistency with observed wind variability.

Overall, the U-Net reconstruction provides a more accurate depiction of 950-hPa winds than ERA5, particularly for meridional flow and high-wind regimes associated with MBLJs. These results demonstrate the value of the satellite-driven machine learning approach for improving low-level wind estimates in offshore regions where in situ observations are sparse.

4.3. MBLJ Characteristics From Reconstructed Wind Fields

Following independent validation against shipborne LiDAR observations, the trained U-Net model was driven by the HY-2B sea surface wind data set from July 2019 to December 2023 to reconstruct 950-hPa wind fields. For the same period, MBLJ events were identified from ERA5 using the criteria described in Section 3.4, yielding a total

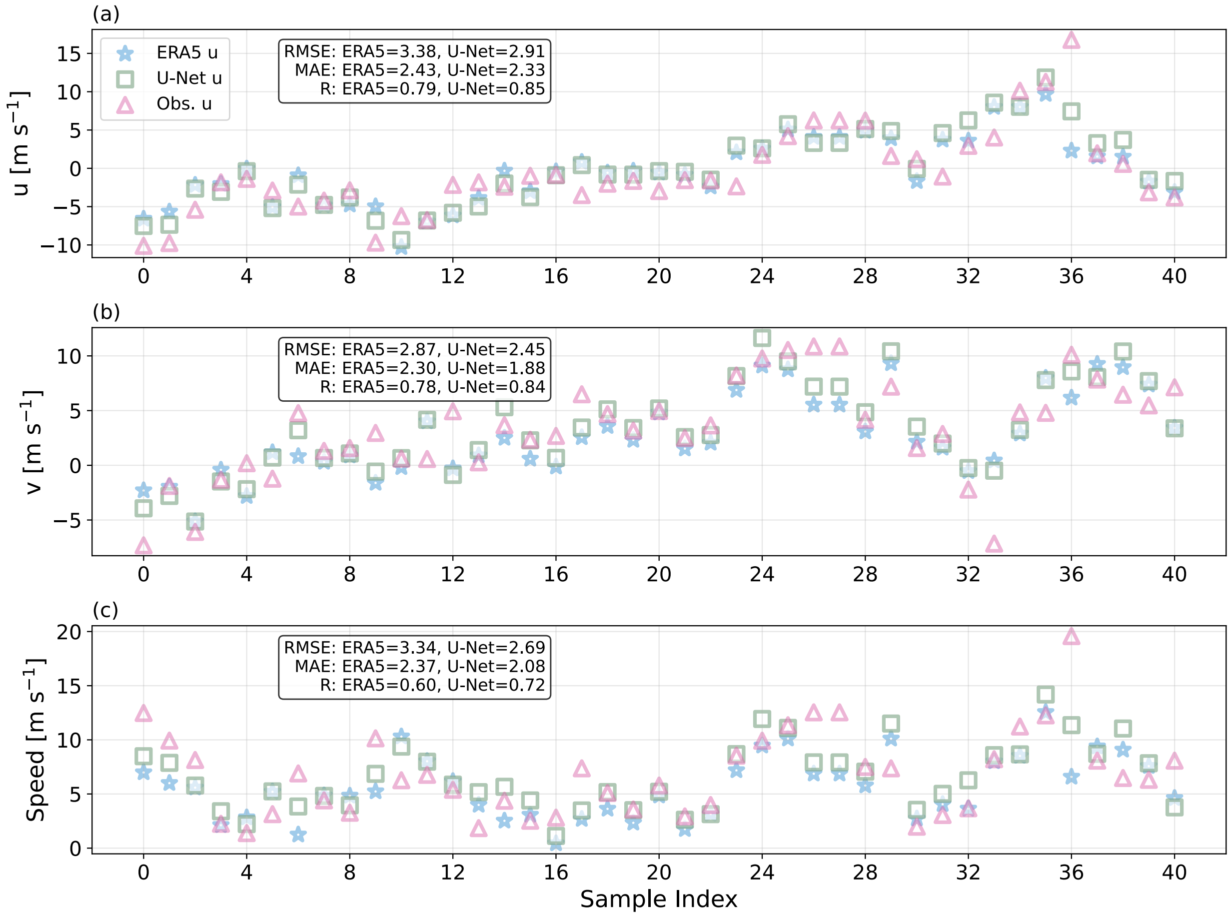

Figure 3. Comparisons of 950-hPa winds from the U-Net reconstruction, ERA5 reanalysis, and ship-based LiDAR observations for (a) *u* component, (b) *v* component, and (c) wind speed.

of 105 events. The reconstructed MBLJs based on satellite inputs were then compared with their ERA5 counterparts to assess differences in jet intensity and spatial structure.

Figure 4 shows that the satellite-based model outputs (SAT) generally produce stronger and more spatially extensive MBLJs than ERA5. Event-mean wind speeds at 950 hPa, defined as the spatial average over the MBLJ region for each snapshot associated with an identified event, are larger in SAT for nearly all events, with a mean

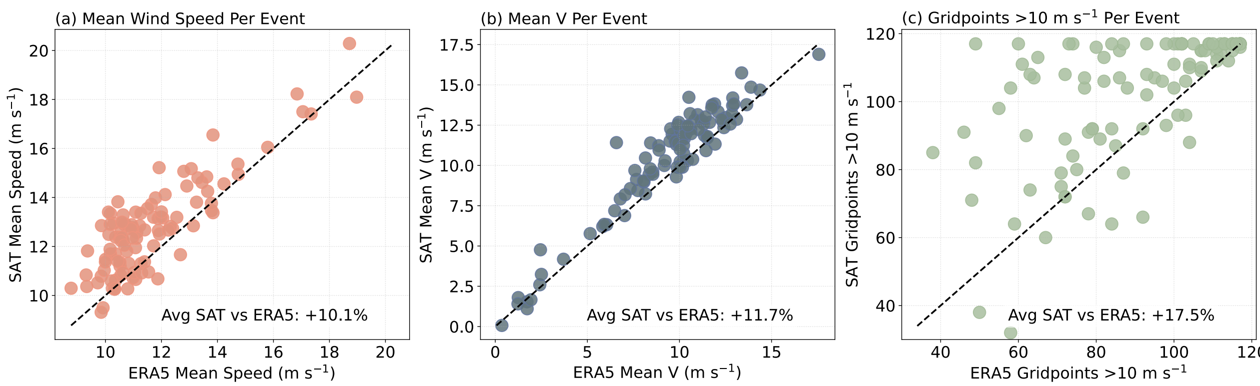

Figure 4. Comparisons of MBLJ characteristics derived from HY-2B-driven reconstructions (SAT) and ERA5 reanalysis for 105 identified MBLJ events: (a) event-mean wind speed, (b) event-mean meridional wind, and (c) the number of grid points with wind speeds exceeding 10 m s^{-1} within the MBLJ domain (18°–21°N, 111°–113°E). Each point represents one event. The dashed line denotes the 1:1 reference.

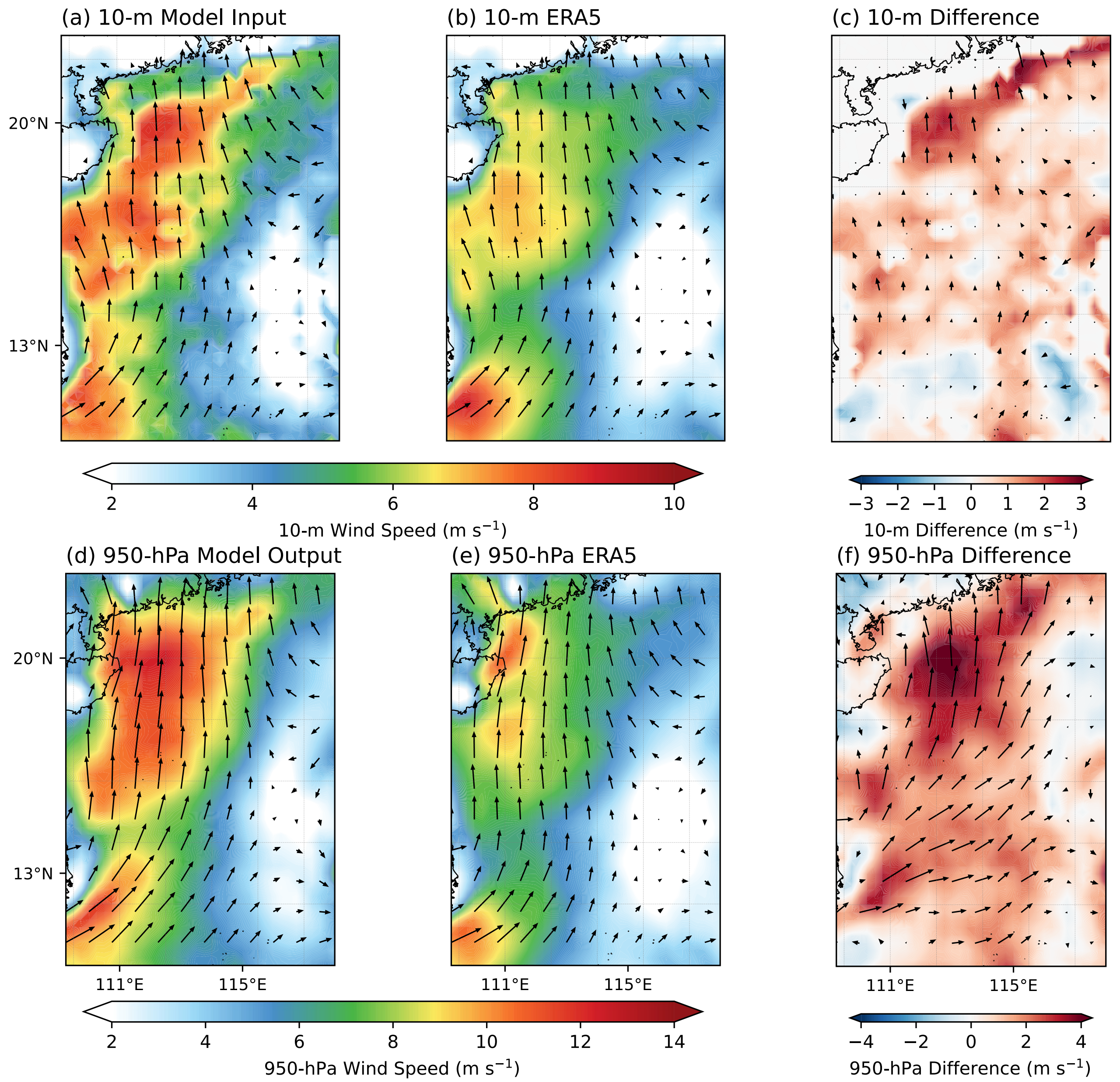

Figure 5. Comparison of surface and 950-hPa wind fields for a representative MBLJ event. Panels (a)–(c) show the 10-m winds from the satellite-based model input, ERA5, and their difference (SAT minus ERA5), respectively. Panels (d)–(f) present the corresponding 950-hPa winds from the model output, ERA5, and their difference. Shading indicates wind speed (m s^{-1}), and vectors denote horizontal wind direction.

enhancement of about 10.1%, indicating a systematic intensification of the reconstructed jets. The meridional wind component exhibits a similar behavior, with SAT values exceeding those of ERA5 by approximately 11.7%, while retaining comparable event-to-event variability. This enhancement suggests that the reconstruction more effectively captures the southerly momentum surges characteristic of MBLJs over the northern South China Sea.

Differences are also evident in the jet spatial extent. The SAT identifies a larger area with wind speeds exceeding 10 m s^{-1} within the MBLJ detection domain, yielding a mean increase of 17.5% in the number of grid points relative to ERA5. Although MBLJ identification requires that more than 50% of the domain satisfy the jet criteria, some ERA5 events display fewer than 59 grid points (50% of the detection domain) above the 10 m s^{-1} threshold in Figure 4. This discrepancy arises because the detection algorithm considers the maximum wind within the

10.1029/2026GL122115

lowest 100-hPa layer, whereas Figure 4 compares winds strictly at 950 hPa. Consequently, ERA5 may slightly underestimate jet extent when the maximum winds occur below 950 hPa.

To illustrate the structural differences, Figure 5 shows a representative MBLJ event. At the sea surface, the satellite-based model input shows a well-organized southwesterly jet core extending from the central basin toward the northern shelf, whereas ERA5 exhibits a weaker and smoother flow. Positive differences of 0.5–2 m s^{-1} along the jet axis highlight ERA5's underestimation of near-surface wind speeds. This improvement becomes more pronounced at 950 hPa: the U-Net reconstruction yields a broader and more intense jet core than ERA5, with positive differences frequently reaching 1–3 m s^{-1}. The largest enhancements occur over the continental shelf and offshore Guangdong and Hainan, aligning well with the intensified sea surface winds.

Despite the use of merged surface wind inputs near the coast, the reconstructed 950-hPa wind field remains spatially coherent and does not exhibit spurious small-scale convergence features (Figures 5a and 5d), indicating that the model suppresses discontinuities in the input rather than directly propagating them. In addition, the enhanced 950-hPa winds do not always coincide exactly with the surface wind maxima and can extend into adjacent regions where the surface wind field is partly filled with reanalysis data. Such spatial offsets, also evident in the reanalysis data set (Figures 5b and 5e), reflect the dynamical adjustment between surface winds and boundary-layer circulation, rather than artifacts introduced by the merged input.

Overall, the satellite-driven reconstruction produces MBLJs that are stronger and broader than those represented in ERA5. These results suggest that satellite-driven machine learning reconstruction can effectively mitigate the systematic underestimation of MBLJ intensity and spatial extent in reanalysis products, particularly in data-sparse marine environments.

5. Conclusions

This study develops a deep learning framework to reconstruct marine boundary layer jets (MBLJs) over the northern South China Sea using satellite-derived sea surface winds. A U-Net model, trained on multi-decadal ERA5 data, is driven by HY-2B scatterometer observations to generate 950-hPa wind fields, corresponding to typical MBLJ heights. Validation against independent measurements demonstrates that the reconstructed winds substantially reduce errors relative to ERA5, particularly for the meridional (v) component and total wind speed. Specifically, RMSE and MAE for v decrease from 2.87 and 2.30 m s^{-1} to 2.45 m s^{-1} and 1.88 m s^{-1}. For total wind speed, RMSE and MAE values decrease from 3.34 and 2.37 m s^{-1} to 2.69 and 2.08 m s^{-1}, indicating improved capture of meridional variability and jet intensity. The reconstructed winds also enhance the spatial extent of MBLJs. Jet-event-based evaluations using HY-2B data from 2019 to 2023 further show that the satellite-driven reconstruction systematically strengthens and expands MBLJs, effectively mitigating the longstanding underestimation of jet strength in reanalysis products over this data-sparse marine region. Although MBLJs occur predominantly during the warm season, sensitivity experiments show that restricting training to warm-season samples does not improve performance (not shown). In the warm-season-only experiment, the reconstruction skill for zonal wind and wind speed remains comparable, whereas the meridional wind error increases. This highlights the importance of using year-round data to provide diverse dynamical constraints and improve the model's generalization, leading to more robust and physically consistent reconstructions.

The primary innovation of this study is the integration of satellite sea surface wind observations with a machine-learning–based vertical reconstruction approach to recover MBLJ structures poorly represented in reanalysis. By leveraging sea surface winds to infer boundary-layer winds, this framework offers a practical pathway for improving low-level wind analyses in regions lacking direct observations. The approach shows promise for enhancing operational analyses, advancing understanding of MBLJ-related heavy rainfall, and supporting future data assimilation systems that combine satellite winds with ML-based vertical inference.

Several limitations highlight opportunities for future research. Relying on a single scatterometer platform (HY-2B) inevitably constrains temporal coverage. Incorporating additional satellites such as HY-2C/D and Fengyun-series scatterometers would enhance both sampling frequency and reconstruction robustness. Moreover, the current framework focuses on wind reconstruction at a single pressure level (950 hPa). Although many MBLJs peak near this height, others may occur at 975 or 925 hPa. Extending the model to three-dimensional boundary-layer wind fields would enable a more complete depiction of vertical variability and jet evolution. Additionally, scatterometer winds remain vulnerable to rain contamination. The integration of Synthetic Aperture Radar

(SAR)-derived winds and other satellite observations could further improve low-level wind quality and the realism of reconstructed MBLJ features.

Conflict of Interest

The authors declare no conflicts of interest relevant to this study.

Availability Statement

The ERA5 reanalysis data were obtained from ECMWF via https://cds.climate.copernicus.eu/datasets/reanalysis-era5-pressure-levels?tab=overview (Hersbach et al., 2018). The HY-2B sea surface wind fields used as input, the corresponding 950-hPa winds and LiDAR data are available at Zenodo (Y. Lin et al., 2026).

Acknowledgments
This study was supported by the Southern Marine Science and Engineering Guangdong Laboratory (Zhuhai) (SML2024SP035, SML2024SP012, and 311024001), the National Natural Science Foundation of China (Grant 42475002), the Guangdong Project of Basic and Applied Basic Research (Grants 2024A1515510005 and 2025A1515011974), and the Key Innovation Team of the China Meteorological Administration (CMA2023ZD08). We also acknowledge the high-performance computing support from School of Atmospheric Sciences of Sun Yat-sen University.

References

Atlas, R., Hoffman, R., Leidner, S., Sienkiewicz, J., Yu, T.-W., Bloom, S., et al. (2001). The effects of marine winds from scatterometer data on weather analysis and forecasting. *Bulletin of the American Meteorological Society*, *82*(9), 1965–1990. https://doi.org/10.1175/1520-0477(2001)082<1965:teomwf>2.3.co;2

Bi, K., Xie, L., Zhang, H., Chen, X., Gu, X., & Tian, Q. (2023). Accurate medium-range global weather forecasting with 3D neural networks. *Nature*, *619*(7970), 533–538. https://doi.org/10.1038/s41586-023-06185-3

Chang, P., Jelenak, Z., Sienkiewicz, J., Knabb, R., Brennan, M., Long, D., & Freeberg, M. (2009). Operational use and impact of satellite remotely sensed ocean surface vector winds in the marine warning and forecasting environment. *Oceanography*, *22*(2), 194–207. https://doi.org/10.5670/oceanog.2009.49

Chase, R. J., Harrison, D. R., Lackmann, G. M., & McGovern, A. (2023). A machine learning tutorial for operational meteorology. Part II: Neural networks and deep learning. *Weather and Forecasting*, *38*(8), 1271–1293. https://doi.org/10.1175/waf-d-22-0187.1

Chelton, D. B., Freilich, M. H., Sienkiewicz, J. M., & Von Ahn, J. M. (2006). On the use of QuikSCAT scatterometer measurements of surface winds for marine weather prediction. *Monthly Weather Review*, *134*(8), 2055–2071. https://doi.org/10.1175/mwr3179.1

Chen, G., Sha, W., Iwasaki, T., & Wen, Z. (2017). Diurnal cycle of a heavy rainfall corridor over east Asia. *Monthly Weather Review*, *145*(8), 3365–3389. https://doi.org/10.1175/MWR-D-16-0423.1

Du, Y., & Chen, G. (2018). Heavy rainfall associated with double low-level jets over southern China. Part I: Ensemble-based analysis. *Monthly Weather Review*, *146*(11), 3827–3844. https://doi.org/10.1175/MWR-D-18-0101.1

Du, Y., & Chen, G. (2019). Heavy rainfall associated with double low-level jets over southern China. Part II: Convection initiation. *Monthly Weather Review*, *147*(2), 543–565. https://doi.org/10.1175/MWR-D-18-0102.1

Du, Y., & Rotunno, R. (2014). A simple analytical model of the nocturnal low-level jet over the Great Plains of the United States. *Journal of the Atmospheric Sciences*, *71*(10), 3674–3683. https://doi.org/10.1175/jas-d-14-0060.1

Du, Y., Shen, Y., & Chen, G. (2022). Influence of coastal marine boundary layer jets on rainfall in South China. *Advances in Atmospheric Sciences*, *39*(5), 782–801. https://doi.org/10.1007/s00376-021-1195-7

Du, Y., & Yi, S. (2025). The relationship scenarios between boundary layer jet and coastal heavy rainfall during the pre-summer rainy season of South China. *Journal of Meteorological Research*, *39*(1), 26–40. https://doi.org/10.1007/s13351-025-4138-x

Fetterer, F., Gineris, D., & Wackerman, C. C. (2002). Validating a scatterometer wind algorithm for ERS-1 SAR. *IEEE Transactions on Geoscience and Remote Sensing*, *36*(2), 479–492. https://doi.org/10.1109/36.662731

Fu, D., Du, Y., Mai, C., Li, M., & Li, C. (2025). Impact of boundary layer jets on cold pool characteristics observed from the 356-m high Shenzhen Meteorological Tower. *Journal of Geophysical Research: Atmospheres*, *130*(19), e2024JD042926. https://doi.org/10.1029/2024jd042926

Gu, J., Wang, Z., Kuen, J., Ma, L., Shahroudy, A., Shuai, B., et al. (2018). Recent advances in convolutional neural networks. *Pattern Recognition*, *77*, 354–377. https://doi.org/10.1016/j.patcog.2017.10.013

Hersbach, H., Bell, B., Berrisford, P., Biavati, G., Horányi, A., Muñoz Sabater, J., et al. (2018). ERA5 hourly data on pressure levels from 1979 to present [Dataset]. *Copernicus Climate Change Service (C3S) Climate Data Store (CDS)*. https://doi.org/10.24381/cds.bd0915c6

LeCun, Y., & Bengio, Y. (1998). *Convolutional networks for images, speech, and time series*. The Handbook of Brain Theory and Neural Networks. https://doi.org/10.5555/303568.303704

Li, X., Yang, J., Wang, J., & Han, G. (2022). Evaluation and calibration of remotely sensed high winds from the HY-2B/C/D scatterometer in tropical cyclones. *Remote Sensing*, *14*(18), 4654. https://doi.org/10.3390/rs14184654

Li, Z., Luo, Y., Du, Y., & Chan, J. C. L. (2020). Statistical characteristics of pre-summer rainfall over South China and associated synoptic conditions. *Journal of the Meteorological Society of Japan. Series II*, *98*(1), 213–233. https://doi.org/10.2151/jmsj.2020-012

Lin, C., Yang, K., Qin, J., & Fu, R. (2013). Observed coherent trends of surface and upper-air wind speed over China since 1960. *Journal of Climate*, *26*(9), 2891–2903. https://doi.org/10.1175/jcli-d-12-00093.1

Lin, M., Zou, J., Xie, X., & Zhang, Y. (2013). HY-2A microwave scatterometer wind retrieval algorithm. *Engineering and Science*, *68*, 68–74.

Lin, Y., & Du, Y. (2025). Sensitivity of coastal rainfall simulation to the assimilation of wind profiles near the marine boundary layer jet: An observing system simulation experiment. *Journal of Geophysical Research: Atmospheres*, *130*(15), e2025JD044106. https://doi.org/10.1029/2025jd044106

Lin, Y., Du, Y., & Wang, J. (2026). Satellite and LiDAR data [Dataset]. *Zenodo*. https://doi.org/10.5281/ZENODO.18371490

Lukens, K. E., Ide, K., Garrett, K., Liu, H., Santek, D., Hoover, B., & Hoffman, R. N. (2022). Exploiting Aeolus level-2b winds to better characterize atmospheric motion vector bias and uncertainty. *Atmospheric Measurement Techniques*, *15*(9), 2719–2743. https://doi.org/10.5194/amt-15-2719-2022

Luo, Y., & Du, Y. (2023). The roles of low-level jets in "21·7" Henan extremely persistent heavy rainfall event. *Advances in Atmospheric Sciences*, *40*(3), 350–373. https://doi.org/10.1007/s00376-022-2026-1

Ma, Z., Li, J., Han, W., Li, Z., Zeng, Q., Menzel, W. P., et al. (2021). Four-dimensional wind fields from geostationary hyperspectral infrared sounder radiance measurements with high temporal resolution. *Geophysical Research Letters*, *48*(14), e2021GL093794. https://doi.org/10.1029/2021GL093794

Mears, C., Lee, T., Ricciardulli, L., Wang, X., & Wentz, F. (2022). Improving the accuracy of the cross-calibrated multi-platform (CCMP) ocean vector winds. *Remote Sensing*, *14*(17), 4230. https://doi.org/10.3390/rs14174230

Ronneberger, O., Fischer, P., & Brox, T. (2015). U-Net: Convolutional networks for biomedical image segmentation. In N. Navab, J. Hornegger, W. M. Wells, & A. F. Frangi (Eds.), *Medical Image Computing and Computer-Assisted Intervention—MICCAI 2015* (pp. 234–241). Springer International Publishing. https://doi.org/10.1007/978-3-319-24574-4_28

Shreffler, J. H. (1982). Intercomparisons of upper air and surface winds in an urban region. *Boundary-Layer Meteorology*, *24*(3), 345–356. https://doi.org/10.1007/bf00121599

Stensrud, D. J. (1996). Importance of low-level jets to climate: A review. *Journal of Climate*, *9*(8), 1698–1711. https://doi.org/10.1175/1520-0442(1996)009<1698:iolljt>2.0.co;2

Sun, X., Zhong, X., Xu, X., Huang, Y., Li, H., Neelin, J. D., et al. (2025). A data-to-forecast machine learning system for global weather. *Nature Communications*, *16*(1), 6658. https://doi.org/10.1038/s41467-025-62024-1

Tu, C.-C., Chen, Y.-L., Lin, P.-L., & Du, Y. (2019). Characteristics of the marine boundary layer jet over the South China Sea during the early summer rainy season of Taiwan. *Monthly Weather Review*, *147*(2), 457–475. https://doi.org/10.1175/mwr-d-18-0230.1

Velden, C. S., & Bedka, K. M. (2009). Identifying the uncertainty in determining satellite-derived atmospheric motion vector height attribution. *Journal of Applied Meteorology and Climatology*, *48*(3), 450–463. https://doi.org/10.1175/2008jamc1957.1

Wang, X., Liu, L., Shi, H., Dong, X., & Zhu, D. (2012). In-orbit calibration and performance evaluation of HY-2 scatterometer. In *2012 IEEE International Geoscience and Remote Sensing Symposium* (pp. 4614–4616). https://doi.org/10.1109/IGARSS.2012.6350438

Wang, Z., Zou, J., Stoffelen, A., Lin, W., Verhoef, A., Li, X., et al. (2021). Scatterometer sea surface wind product validation for HY-2C. *IEEE Journal of Selected Topics in Applied Earth Observations and Remote Sensing*, *14*, 6156–6164. https://doi.org/10.1109/jstars.2021.3087742

Witschas, B., Lemmerz, C., Geiß, A., Lux, O., Marksteiner, U., Rahm, S., et al. (2020). First validation of Aeolus wind observations by airborne Doppler wind LiDAR measurements. *Atmospheric Measurement Techniques*, *13*(5), 2381–2396. https://doi.org/10.5194/amt-13-2381-2020

Xie, H., Xu, Q., Cheng, Y., Yin, X., & Jia, Y. (2022). Reconstruction of subsurface temperature field in the South China Sea from satellite observations based on an attention U-Net model. *IEEE Transactions on Geoscience and Remote Sensing*, *60*, 1–19. https://doi.org/10.1109/TGRS.2022.3200545

Xing, J., Shi, J., Lei, Y., Huang, X.-Y., & Liu, Z. (2016). Evaluation of HY-2A scatterometer wind vectors using data from buoys, ERA-interim and ASCAT during 2012–2014. *Remote Sensing*, *8*(5), 390. https://doi.org/10.3390/rs8050390

Yang, H., Du, Y., & Sun, J. (2025). The merger of a supercell and squall line in the Great Plains. 1: Initiation of the supercell. *Journal of Geophysical Research: Atmospheres*, *130*(13), e2024JD042393. https://doi.org/10.1029/2024jd042393

Yang, X., Li, X., Pichel, W. G., & Li, Z. (2011). Comparison of ocean surface winds from ENVISAT ASAR, MetOp ASCAT scatterometer, buoy measurements, and NOGAPS model. *IEEE Transactions on Geoscience and Remote Sensing*, *49*(12), 4743–4750. https://doi.org/10.1109/tgrs.2011.2159802

Zhang, M., & Meng, Z. (2019). Warm-sector heavy rainfall in southern China and its WRF simulation evaluation: A low-level-jet perspective. *Monthly Weather Review*, *147*(12), 4461–4480. https://doi.org/10.1175/mwr-d-19-0110.1

Zhang, X., Luo, Y., & Du, Y. (2024). Observation of boundary-layer jets in the northern South China Sea by a research vessel. *Remote Sensing*, *16*(20), 3872. https://doi.org/10.3390/rs16203872